Equilibrium Melting Temperature of Isotactic Polypropylene with High Tacticity. 2. Determination by Optical Microscopy

Koji Yamada,*,† Masamichi Hikosaka,‡ Akihiko Toda,‡ Shinichi Yamazaki,‡ and Katsuharu Tagashira†

Kawasaki Development Center, SunAllomer Limited, 2−3−2 Yako, Kawasaki-ku, Kawasaki 210-8548, Japan, and Faculty of Integrated Arts and Sciences, Hiroshima University, 1-7-1 Kagamiyama, Higashi-Hiroshima 739-8521, Japan

Received July 26, 2002; Revised Manuscript Received February 24, 2003

ABSTRACT: In part 1 of this series, we proposed a new method to determine the correct equilibrium melting temperature (T_m^0). Effects of the "melting kinetics" and lamellar thickening were omitted from T_m. The correct T_m^0 of isotactic polypropylene (iPP) ([*mmmm*] = 99.6%, $M_n = 64 \times 10^3$, and $M_w/M_n = 2.4$) was observed to be 186.1 °C. In this paper, the rigorous Gibbs−Thomson plot was obtained by using the direct correspondence between maximum melting temperature ($T_{m,max}$) and maximum lamellar thickness (l_{max}). $T_{m,max}$ and l_{max} were observed by means of optical microscope and transmission electron microscope (TEM), respectively. The validity of the Gibbs−Thomson plot obtained by means of a differential scanning calorimeter (DSC) (part 1 of this series) was confirmed by comparing it with the rigorous Gibbs−Thomson plot in this paper. The Hoffman−Weeks plot is widely used as one of the methods to obtain T_m^0. It was shown that the Hoffman−Weeks plot is correct only when $l \propto 1/\Delta T$, where ΔT is the degree of supercooling, is satisfied. However, in the case of iPP, the condition is not satisfied, and so the result obtained by the Gibbs−Thomson plot is not equivalent to that obtained by the Hoffman−Weeks plot. The existence of α2′ phase was confirmed again by breakings in slopes of l and T_m against T_c at 159 °C. Furthermore, the broad bimodal distribution of l was caused by the difference between the lamellar thickening growth rate of isolated mother lamellae and the lamellae thickening rate of stacked daughter lamellae.

1. Introduction

In the previous paper (part 1), a new method to determine a reliable equilibrium melting temperature (T_m^0) was proposed.[1] In the method, the Gibbs−Thomson plot

$$T_m(l) = T_m^0 - \frac{C}{l} \tag{1}$$

was applied, where l is lamellar thickness, $T_m(l)$ is melting temperature (T_m) of lamella with l and C is given by eq 1 in part 1 of this series.[2] It was shown that two effects depending on heating rate (β), i.e., the "melting kinetics" and lamellar thickening, should be omitted from $T_m(l)$.

In part 1, the differential scanning calorimeter (DSC) and the transmission electron microscope (TEM) were used for observations of $T_m(l)$ and l, respectively. It was shown that endothermic peak temperature (T_m(DSC)) corresponds to reciprocal averaged lamellar thickness ($\langle l^{-1} \rangle$) in the Gibbs−Thomson equation. T_m^0 of isotactic polypropylene (iPP) was determined to be 186.2 °C.

DSC measurement is convenient and useful to observe T_m. However, there is a problem that the Gibbs−Thomson plot made by using T_m(DSC) is not always rigorous for polymers, because the correspondence between T_m(DSC) and $\langle l^{-1} \rangle$ is reliable only when distribution of l ($f(l)$) and that of T_m are sharp, and not when they are broad. It is usual in polymers that $f(l)$ is rather wide.[3]

In this paper (part 2), a "rigorous Gibbs−Thomson plot" will be carried out by using direct correspondence between T_m and l^{-1}, i.e., maximum T_m ($T_{m,max}$) and maximum l (l_{max}), which can be observed by means of an optical microscope and TEM, respectively. The fractionated iPP used in part 1 was used in this study. Comparison between "the rigorous Gibbs−Thomson plot" and a convenient Gibbs−Thomson plot obtained by using DSC will be able to evaluate the validity of the latter one.

1.1. Effect of "Melting Kinetics" and Lamellar Thickening on T_m. In part 1 of this series, it was proposed that correct $T_m(l)$ can be obtained by omitting the two effects of the "melting kinetics" and lamellar thickening on T_m.[4−7] The effect of lamellar thickening can be omitted when l is thick enough, such as $l > 15$ nm for iPP. The effect of the "melting kinetics" of thick lamellae can be omitted by observation of isothermal melting. Therefore, the $T_{m,max}$ of thick lamella with $l >$ 20 nm would be directly observed by means of an optical microscope in this paper.

1.2. Significant Lamellar Thickening in the Mobile Phase of iPP. Thick lamellae can be obtained by isothermal crystallization at high T_c. Hikosaka et al. proposed a chain sliding diffusion theory that lamellae thicken significantly when polymers are crystallized in mobile phases such as the hexagonal phase, a liquid crystalline phase, or a kind of disordered phase where the lattice is expanded and chains are packed loosely.[8−10]

The α2′ phase of iPP above $T_{\alpha 2-\alpha 2'} = 159$ °C is a mobile phase, where $T_{\alpha 2-\alpha 2'}$ is the α2−α2′ transition temperature.[1,11,12] Lamellar thickening should be accelerated significantly in the mobile phase. In the present paper, it will be confirmed that significant thick lamellae are formed in the α2′ phase.

1.3. Melting Behavior and Lamellar Morphology of iPP. The melting behavior of spherulite should be closely related to change in lamellar morphology. There

* Corresponding author.
† SunAllomer Ltd.
‡ Hiroshima University.

10.1021/ma021207a CCC: $25.00
Published on Web 06/04/2003

is no crosshatching lamellae when iPP is crystallized at a higher T_c than 150 °C.[13−19] In part 1 of this series, we suggested that the two-stage melting endotherm of iPP crystallized at $T_c \geq 148$ °C observed by means of DSC corresponds to the bimodal distribution of l. In this paper, detailed evidences of the bimodal distribution of l will be shown by means of TEM, corresponding to a change of the optical morphology of spherulites.

1.4, Problem of the Hoffman—Weeks Plot. The Hoffman−Weeks plot method has been widely used to obtain T_m^0 of polymers.[20−22] Hoffman and Weeks assumed that,

$$l = \beta l^* \propto \frac{1}{\Delta T} \tag{2a}$$

$$l = \text{constant} \quad \text{(on heating)} \tag{2b}$$

where β is a constant, l^* is l of a critical nucleus, and ΔT is the degree of supercooling. By application of these assumptions to the Gibbs−Thomson equation, the following equation is obtained

$$T_m = bT_c + c \tag{3a}$$

$$c = (1 - b)T_m^0 \tag{3b}$$

where b and c are constants. T_m^0 can be obtained as an intersection of lines of $T_m = T_c$ and eq 3a. The Gibbs−Thomson equation (eq 1) is equivalent to the Hoffman−Weeks equation (eq 3a) under the assumptions of eq 2, parts a and b.

T_m^0 obtained from the Hoffman−Weeks plot and that obtained from the Gibbs−Thomson plot are sometimes similar and, however, sometimes quite different. A typical example of the former is polyethylene (PE) and the one of the latter is iPP. [21−28] Furthermore, in the case of polyvinylidenefluoride (PVDF), the Hoffman−Weeks plot cannot give T_m^0.[29,30]

The problem that the Hoffman−Weeks plot does not always work well has not been solved yet. The reason should be that above assumptions are not correct for all polymers. It is possible that l is constant on heating (eq 2b) by using thick lamellae. Therefore, the validity of the Hoffman−Weeks plot method depends on whether eq 2a is satisfied or not. In this paper, the actual validity of the Hoffman−Weeks plot will be tested for typical cases, such as PE and iPP.

1.5. Purpose of This Study. The first purpose is to obtain the correct T_m^0 by using direct correspondence between $T_{m,max}$ and l_{max}^{-1} in the rigorous Gibbs−Thomson plot. $T_{m,max}$ and l_{max}^{-1} will be obtained from the results by means of optical microscope and TEM, respectively. The effect of the "melting kinetics" on T_m was directly omitted by applying isothermal melting condition ($\beta \cong 0$ K/min). Lamellar thickening was also omitted by observing thick lamellae larger than 20 nm. The validity of the convenient Gibbs−Thomson plot by means of DSC in part 1 of this series will be evaluated by comparing both results.

The second purpose is to show that significant lamellar thickening occurs when iPP crystallizes in the α2′ form. Accordingly, it will be confirmed that the α2′ phase of iPP is a kind of mobile phase.

The third purpose is to show that the Hoffman−Weeks plot method is correct only when $l \propto 1/\Delta T$ is satisfied, which will be confirmed from experimental results.

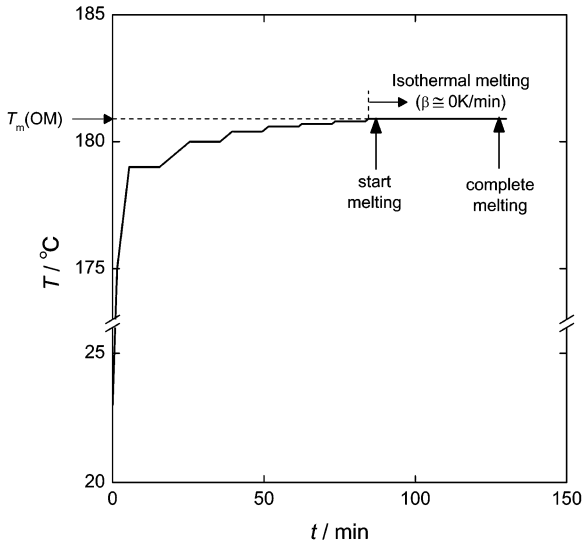

Figure 1. Typical example of a temperature program used to observe T_m(OM) ($=T_{m,max}$) at $\beta \cong 0$ K/min.

2. Experimental Section

2.1. Sample. IPP fraction with high tacticity was used in this study ($M_n = 64 \times 10^3$, $M_w = 152 \times 10^3$, $M_w/M_n = 2.4$ and [*mmmm*] = 99.6%). Isothermal crystallization was carried out at T_c = 148∼166 °C in an oil bath for sufficient time to crystallize completely. To omit the effects of lamellar thickening and melt-recrystallization, thick lamellae crystallized at $T_c \geq 148$ °C were used. Therefore, l is a constant on heating. Details of sample preparation were shown in part 1 of this series.[1]

2.2. Observation of Melting Behavior by Optical Microscopy. Isothermal melting behaviors of spherulite were observed by using an optical microscope, Nikon Optiphot, fixed with a hotstage, LINKAM PH-600M, under a nitrogen flow of 50 mL/min. The temperature of the hotstage was calibrated by using melting temperature of standard materials, indium (156.6 °C) and tin (237.6 °C).

The procedure of determination of $T_{m,max}$ was schematically shown in Figure 1. The sample was heated to a temperature that is slightly lower than T_m. After that, temperature increased by step-by-step heating at interval of 0.1 °C. When spherulites started melting slightly, the temperature was maintained and isothermal melting behavior ($\beta \cong 0$ K/min) was observed. $T_{m,max}$ was defined as a temperature where spherulites disappeared completely after a long time, about 30 min. In this paper, $T_{m,max}$ was denoted as T_m(OM).

2.3. TEM Observation of Lamellar Morphology. A quasi-two-dimensional spherulite about 100 μm thick was formed (Figure 2a). The specimen for TEM observation was cut out from a spherulite indicated as A in order to obtain the correct l of edge-on lamellae. The size of the specimen was about 100 μm × 200 μm × 100 μm (Figure 2b). The specimens embedded in epoxy resin were trimmed with a microtome, Reichert-Nissei Ultracut N, equipped with a glass knife and a trimming knife. The trimmed specimens were exposed to the vapor of ruthenium tetraoxide in a sealed flask at 35 °C for 5 h. After staining, ultrathin sections of about 60 nm thickness were obtained by using a Diatone diamond knife from the center portion, about 50 μm in depth of the specimen surface. The cutting speed was 0.6−1.0 mm/s. The ultrathin sections obtained were supported on a grid 100-mesh and then dried in a desiccator. The morphology of edge-on lamellae was observed by means of TEM, HITACHI H-800, with 150 kV accelerate voltage. To obtain the statistical distribution of l, $f(l)$, l was measured on a lot of edge-on lamellae in several tens of transmission electron micrographs.

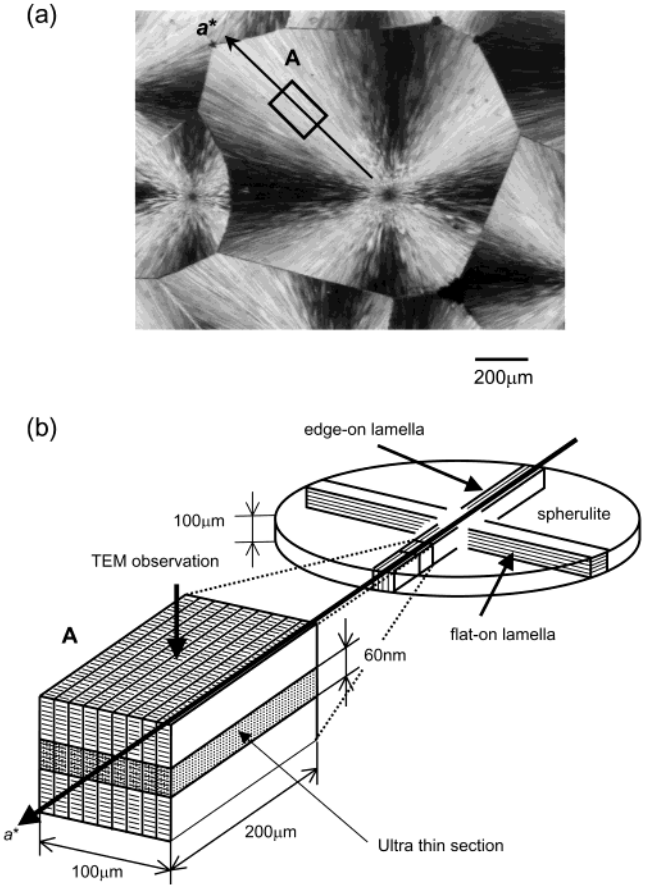

Figure 2. (a) Portion of a spherulite for TEM observation. (b) Schematic illustration of a portion of an ultrathin section in a spherulite.

2.4. Partial Melting. DSC showed double melting endotherms.[1] To confirm that a higher DSC peak (T_m(I)) and a lower peak (T_m(II)) correspond to the melting of thick and thin lamellae, annealing was carried out. DSC measurement was carried out by using Perkin-Elmer DSC7 under nitrogen flow. The details of the DSC measurement were shown in part 1 of this series.[1] The sample was heated to an annealing temperature between T_m(II) and T_m(I) in an oil bath at a heating rate of 5 K/min. The sample temperature was directly measured by thermocouples. When sample temperature strictly reached to the annealing temperature between T_m(II) and T_m(I), the sample was quickly transferred into frozen acetone and quenched.

3. Results

3.1. Comparison of Nonisothermal Melting Behavior Observed by Optical Microscopy and DSC. In part 1 of this series, the DSC melting endotherm showed two-stage melting, i.e., peaks II ($T_{m,\alpha 2'}$(II)) and I ($T_{m,\alpha 2'}$(I)) at low and high temperatures, respectively. It was shown that peaks II and I correspond to meltings of thin and thick lamellae, respectively. To make clear what kind of lamella melts corresponding to DSC peaks, change of optical morphology was observed on heating at $\beta = 5$ K/min.

Typical melting behaviors of a spherulite crystallized at $T_c = 153$ °C $\leq T_{\alpha 2-\alpha 2'}$ and $T_c = 164$ °C $> T_{\alpha 2-\alpha 2'}$ observed by polarized optical microscopy are shown in Figures 3 and 5, and the corresponding DSC curves are shown in Figures 4 and 6, respectively. Parts a, b, c and d in Figures 3 and 5 showed morphologies at the temperatures indicated by arrows a, b, c and d in Figures 4 and 6, respectively.

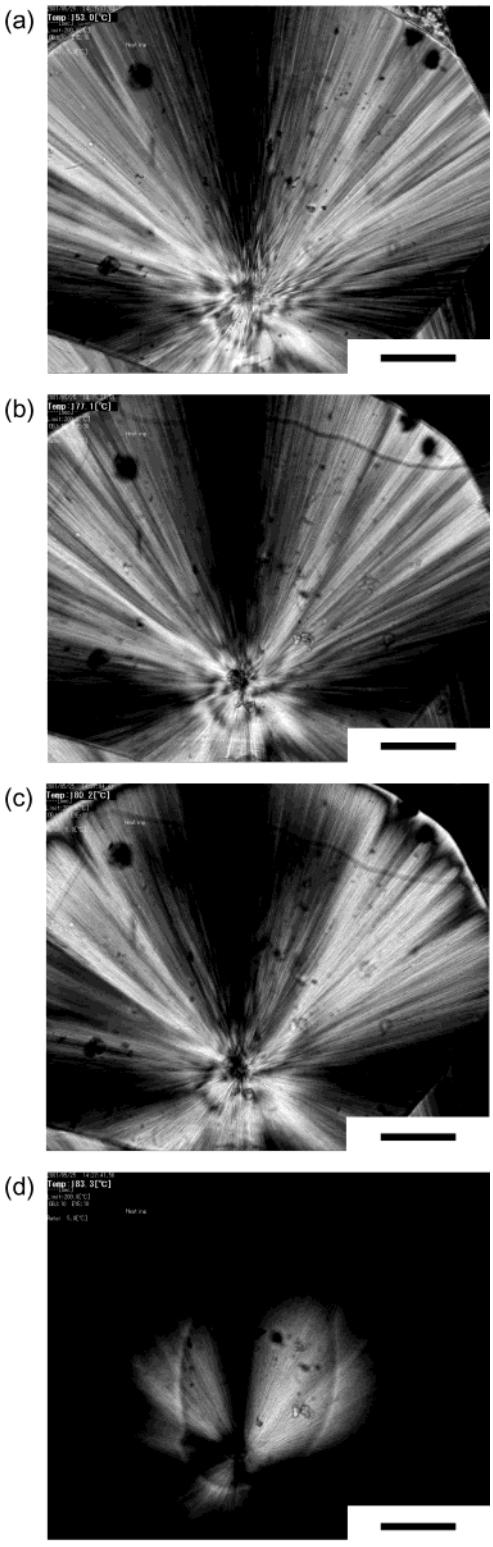

Figure 3. Melting behavior at $\beta = 5$ K/min of iPP spherulite crystallized at $T_c = 153$ °C $< T_{\alpha 2-\alpha 2'} = 159$ °C: (a) 153.0, (b) 177.1, (c) 180.2, and (d) 183.3 °C. Scale bar is 200 μm.

Figure 3a showed morphology before melting. At a little higher temperature (177.1 °C) than $T_{m,\alpha 2'}$(II), fine texture disappeared, which indicated partial melting of thin lamellae (Figure 3b). At $T_{m,\alpha 2'}$(I), 180.2 °C, the distinct texture disappeared and the spherulite melted completely, which indicated complete melting of thick lamellae (Figure 3, parts c and d).

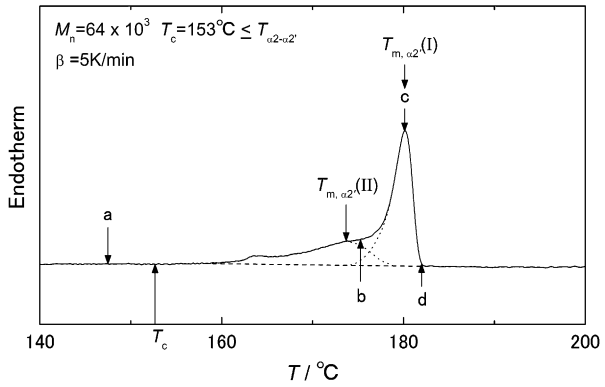

Figure 4. DSC melting curve at $\beta = 5$ K/min of iPP spherulite crystallized at $T_c = 153$ °C ≤ $T_{\alpha2-\alpha2'} = 159$ °C. Parts a, b, c, and d correspond to optical micrographs a, b, c, and d in Figure 3, respectively.

Similar morphological change was observed for the sample crystallized at $T_c = 164$ °C > $T_{\alpha2-\alpha2'}$ (Figures 5). Partial melting (Figure 5b) and whole melting (Figure 5, parts c and d) were observed corresponding to $T_{m,\alpha2'}$(II) and $T_{m,\alpha2'}$(I), respectively (Figure 6).

Thus, it was concluded that the similar "two-stage melting" was observed in the morphological change, as well as in DSC. The partial and complete meltings corresponded to the meltings of thin and thick lamellae, respectively.

3.2. Isothermal Melting Behavior and T_m Observed by Optical Microscopy. Melting behavior of a spherulite was observed by phase contrast optical microscopy under isothermal condition ($\beta \cong 0$ K/min). Two-stage melting behavior was observed for both samples crystallized at $T_c = 153$ °C ≤ $T_{\alpha2-\alpha2'}$ and $T_c = 164$ °C > $T_{\alpha2-\alpha2'}$ (Figures 7 and 8). Figures 7a and 8a showed spherulites before melting. Figures 7b (175.1 °C) and 8b (182.4 °C) showed partial melting, which should correspond to $T_{m,\alpha2'}$(II). Distinct textures were clearly observed. Figures 7c (177.1 °C) and 8c (183.3 °C) showed the start of complete melting. When the spherulites were kept at the same temperatures (Figures 7c and 8c), they melted slowly and disappeared completely (Figures 7d and 8d) after 25 and 30 min, respectively. Therefore, the temperatures of Figure 7d and 8d should correspond to $T_{m,max}$. Thus, $T_{m,max} = T_m$(OM) was obtained to be 177.1 and 183.3 °C for $T_c = 153$ °C ≤ $T_{\alpha2-\alpha2'}$ and $T_c = 164$ °C > $T_{\alpha2-\alpha2'}$, respectively.

3.3. T_c Dependence of $T_{m,\alpha2'}$(OM). T_m(OM) was plotted against T_c in Figure 9. Open symbols indicated T_m(OM) of samples crystallized into the α2 form, and filled symbols indicated that of samples crystallized into the α2′ form. T_m(OM)s of all crystallized specimens were higher than $T_{\alpha2-\alpha2'} = 159$ °C in this study. Therefore, T_m(OM) was denoted as $T_{m,\alpha2'}$(OM).

$T_{m,\alpha2'}$(OM) increased with increasing T_c. Breaking of the differential coefficient (dT_m/dT_c) was observed at 159 °C, which corresponds to the α2−α2′ transition. Therefore, the breaking temperature was

$$T_{\alpha2-\alpha2'}(\mathrm{OM}) = 159\ ^\circ\mathrm{C} \qquad (4)$$

$T_{m,\alpha2'}$(DSC) was also shown as a reference in Figure 9. Both $T_{m,\alpha2'}$(OM) and $T_{m,\alpha2'}$(DSC) at $\beta = 0$ K/min showed similar tendency against T_c, i.e., breakings were observed and the dT_m/dT_c in the α2′ phase was larger than that in the α2 phase. Thus, the α2−α2′ transition was confirmed again.

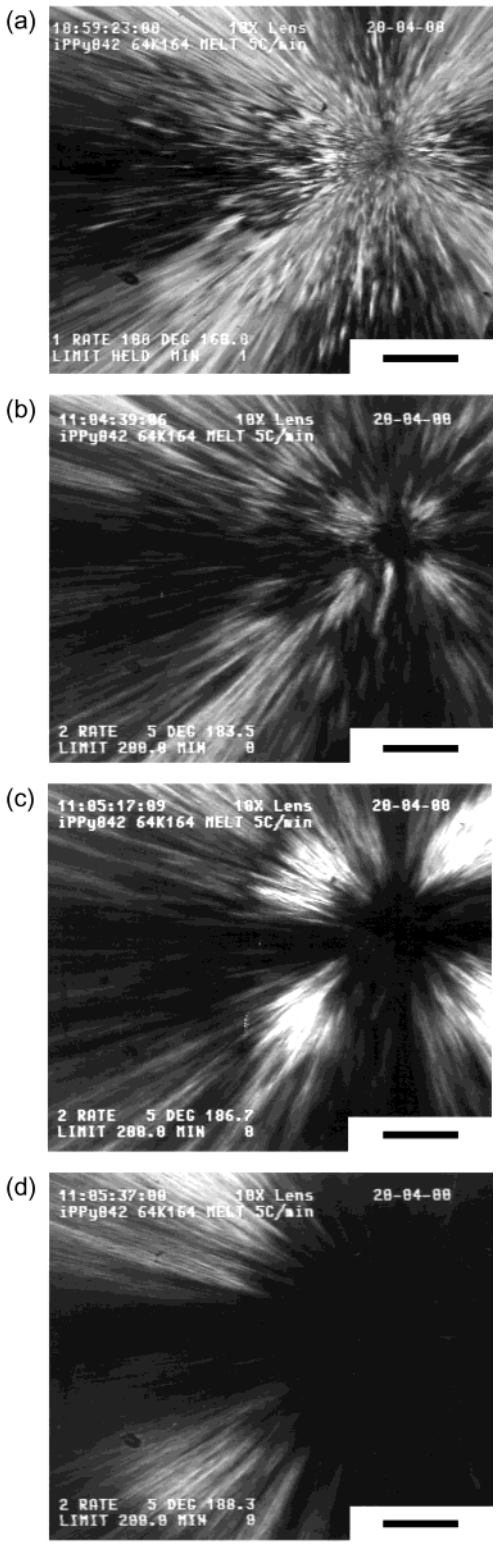

Figure 5. Melting behavior at $\beta = 5$ K/min of iPP spherulite crystallized at $T_c = 164$ °C > $T_{\alpha2-\alpha2'} = 159$ °C: (a) 159.8, (b) 183.3, (c) 186.5, and (d) 188.1 °C. Scale bar is 200 μm.

3.4. Lamellar Morphology and Thickness. Transmission electron micrograph of an ultrathin section with low magnification is shown in Figure 10. The radial direction of the spherulite corresponded to the direction of a^* axis of lamellae. The lateral lengths of the lamellae were several hundreds of micrometers. It corresponds to the texture of spherulite observed by optical microscopy as shown in Figure 2. l was obtained from edge-on

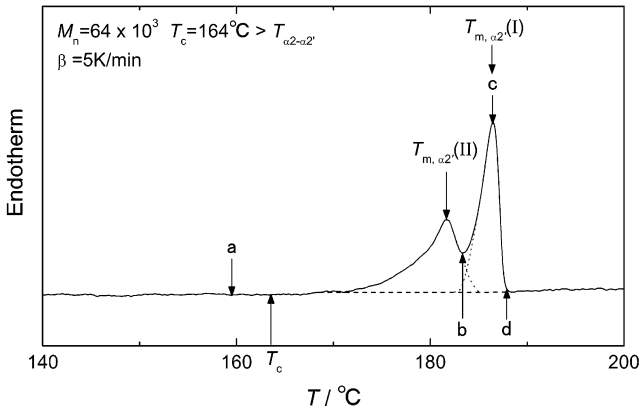

Figure 6. DSC melting curve at $\beta = 5$ K/min of iPP spherulite crystallized at $T_c = 166$ °C > $T_{\alpha2-\alpha2'} = 159$ °C. Parts a, b, c, and d corresponded to optical micrographs a, b, c, and d in Figure 5, respectively.

lamella as indicated by arrows. Crosshatching lamellae were not observed. Typical lamellar morphologies of samples crystallized at $T_c \leq T_{\alpha2-\alpha2'}$ and $T_c > T_{\alpha2-\alpha2'}$ are shown in Figures 11 and 12, respectively.

(a) $T_c \leq T_{\alpha2-\alpha2'}$. Typical transmission electron micrographs of edge-on lamellae crystallized at $T_c = 148$, 153, and 157 °C ≤ $T_{\alpha2-\alpha2'}$ were shown in Figure 11, parts a, b, and c, respectively. Radial direction of spherulite was indicated by an arrow. It was seen that lamellae stacked regularly.

l_{max} indicated by an arrow increased gradually with an increase of T_c. Regions of thick and thin lamellae were observed. They should correspond to DSC peak I and II. Therefore, they were named I and II, respectively. In the case of $T_c = 153$ °C, l of II at the center was 16 nm and that of I at the bottom was 20 nm (Figure 11b).

(b) $T_c > T_{\alpha2-\alpha2'}$. Lamellar morphologies for samples crystallized at $T_c = 162$, 164, and 166 °C were also shown in Figure 12, parts a, b, and c, respectively. l increased significantly, and $f(l)$ became broad with an increase of T_c. In the case of $T_c = 166$ °C, l_{max} reached 70 nm. Regions of thick (I) and thin lamellae (II) were also observed. Stacking became disordered with increase of T_c.

3.5. l_{max} and Distribution of l. Histograms of l for samples crystallized at $T_c \leq T_{\alpha2-\alpha2'}$ and $T_c > T_{\alpha2-\alpha2'}$ are shown in Figures 13 and 14, respectively. Parts a, b and c in Figures 13 and 14 corresponded to parts a, b and c of transmission electron micrographs in Figures 11 and 12, respectively. The scale of the horizontal axis in Figure 13 was the same as that in Figure 14. l_{max} indicated by arrow increased with increase of T_c. The $f(l)$ was estimated as a smoothed curve obtained from histogram. The $f(l)$ was significantly different between $T_c \leq T_{\alpha2-\alpha2'}$ and $T_c > T_{\alpha2-\alpha2'}$.

(a) $T_c \leq T_{\alpha2-\alpha2'}$. For the samples crystallized at $T_c \leq T_{\alpha2-\alpha2'}$, l_{max} increased gradually from 21 to 32 nm with increase of T_c from 148 to 157 °C (Figure 13). $f(l)$ showed bimodal distribution. $f(l)$ was separated into two rather sharp peaks with large l (peak I) and small l (peak II) as indicated by solid curves. $f(l)$ shifted to larger l with increase of T_c.

(b) $T_c > T_{\alpha2-\alpha2'}$. l_{max} of samples crystallized at $T_c > T_{\alpha2-\alpha2'}$ significantly increased from 53 to 69 nm with an increase of T_c from 162 to 166 °C (Figure 14). $f(l)$s also showed bimodal distributions. It was separated into

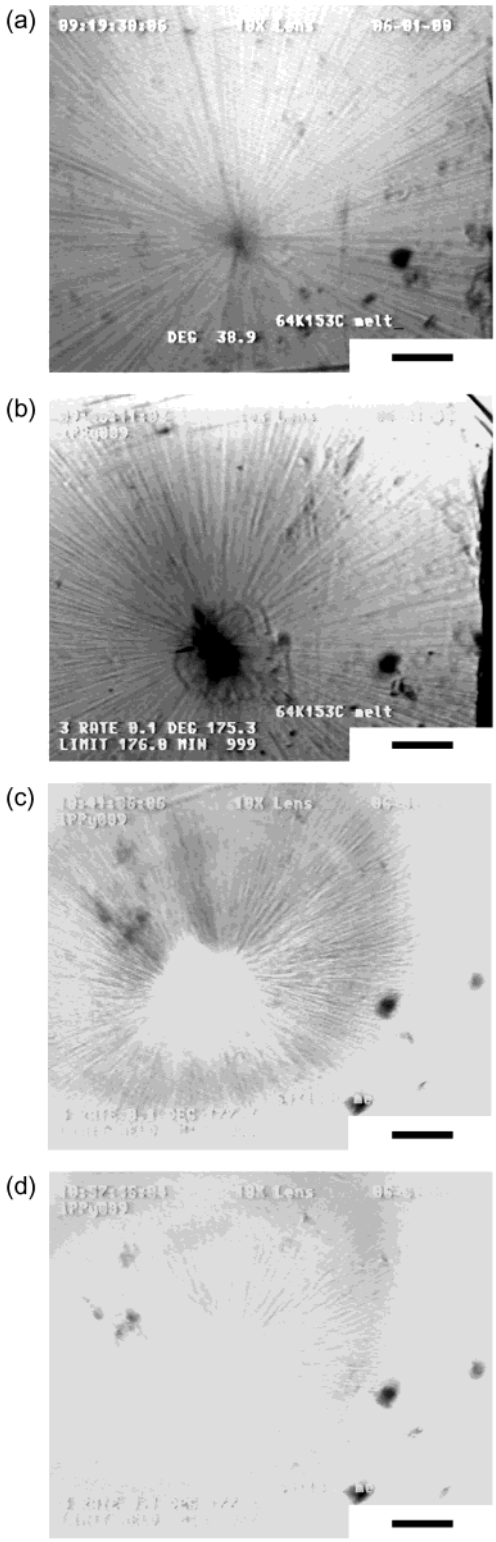

Figure 7. Melting behavior at $\beta \cong 0$ K/min of iPP spherulite crystallized at $T_c = 153$ °C ≤ $T_{\alpha2-\alpha2'} = 159$ °C: (a) room temperature, (b) 175.1 °C, (c) 177.1 °C for 16 min, and (d) 177.1 °C for 32 min. Scale bar is 100 μm.

sharp peak with small l (peak II) and very broad peak with large l (peak I). $f(l)$ of peak I became very broad with increase of T_c. The sharpness of $f(l)$ of peak II did not depend on T_c.

3.6. Confirmation of the Bimodal Distribution of l by Partial Melting. DSC melting curves at heating rate of 5 K/min of sample crystallized at 162 °C is shown

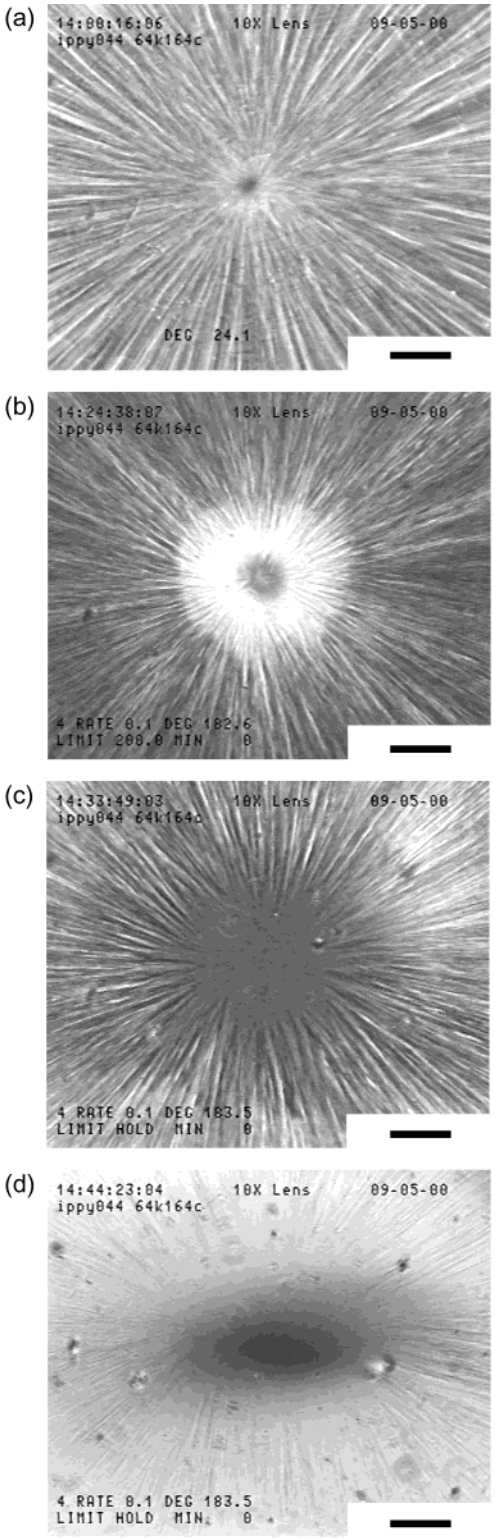

Figure 8. Melting behavior at $\beta \cong 0$ K/min of iPP spherulite crystallized at $T_c = 166$ °C > $T_{\alpha 2-\alpha 2'} = 159$ °C: (a) room temperature, (b) 182.4 °C, (c) 183.3 °C for 0 min, and (d) 183.3 °C for 11 min. Scale bar is 100 μm.

in Figure 15a. The sample temperature reached the annealing temperature, and then the sample was immediately quenched (Figure 15b).

Transmission electron micrographs of the samples before and after annealing are shown in Figure 16, parts a and b, respectively. After annealing, crosshatched very thin lamellae within a spherulite were observed (Figure 16b). It was formed by melt-recrystallization after

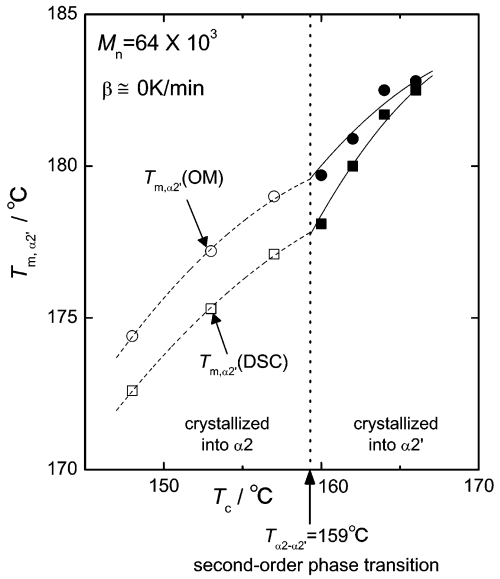

Figure 9. $T_{m,\alpha 2'}$ at $\beta \cong 0$ K/min plotted against T_c. $T_{m,\alpha 2'}$(OM) and $T_{m,\alpha 2'}$(DSC) were indicated by circles and squares, respectively. $T_{m,\alpha 2'}$s of samples crystallized into α2 phase at $T_c \leq T_{\alpha 2-\alpha 2'}$ and α2′ phase at $T_c > T_{\alpha 2-\alpha 2'}$ were indicated by open symbols and filled symbols, respectively.

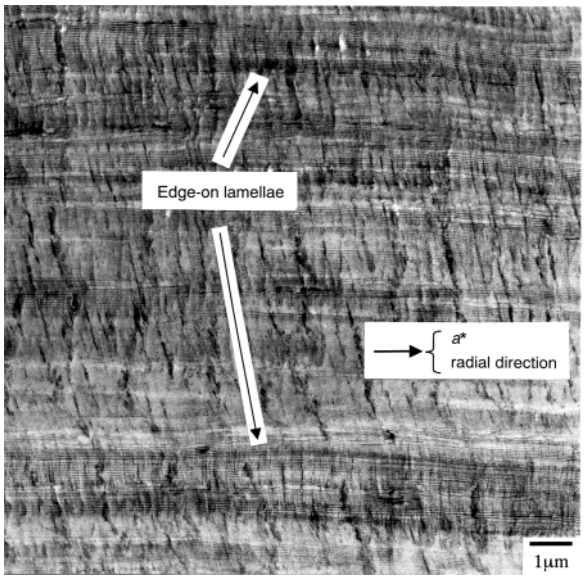

Figure 10. Typical transmission electron micrographs with low magnification of iPP. The horizontal direction corresponds to the radial one of spherulite or *a** axis. Edge-on lamellae were indicated.

partial melting. Thick lamellae were also observed after annealing (Figure 16b), which correspond to thick lamellae of the original sample as indicated by arrow in Figure 16a. The thickness of thick lamellae became slightly thinner due to the disordering of the end surface of lamellae. Corresponding to the morphology change, DSC melting curves of samples after partial melting showed the higher peak (Figure 15c). A melting peak of thin lamellae crystallized at cooling from the annealing temperature also observed. Therefore, the two-stage melting was confirmed by the bimodal distribution of *l*.

3.7. T_c Dependence of l_{max}. l_{max} was plotted against T_c in Figure 17. l_{max} of the specimens crystallized into the α2 form and the α2′ form were indicated by open circles and filled circles, respectively. At $T_c \leq T_{\alpha 2-\alpha 2'}$,

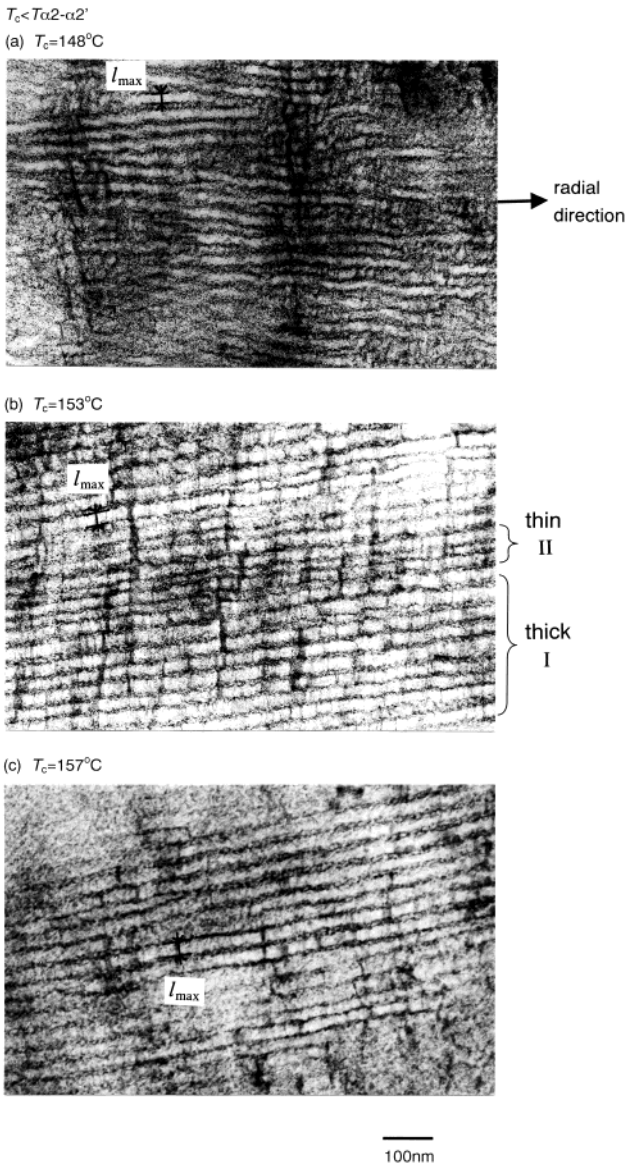

Figure 11. Transmission electron micrographs of lamellar morphology of samples crystallized at $T_c \leq T_{\alpha2-\alpha2'}$: (a) $T_c = 148$, (b) $T_c = 153$, and (c) $T_c = 157$ °C. The horizontal directions were nearly equal to the radial ones of spherulite. Areas of thick lamellae (I) and thin lamellae (II) were indicated.

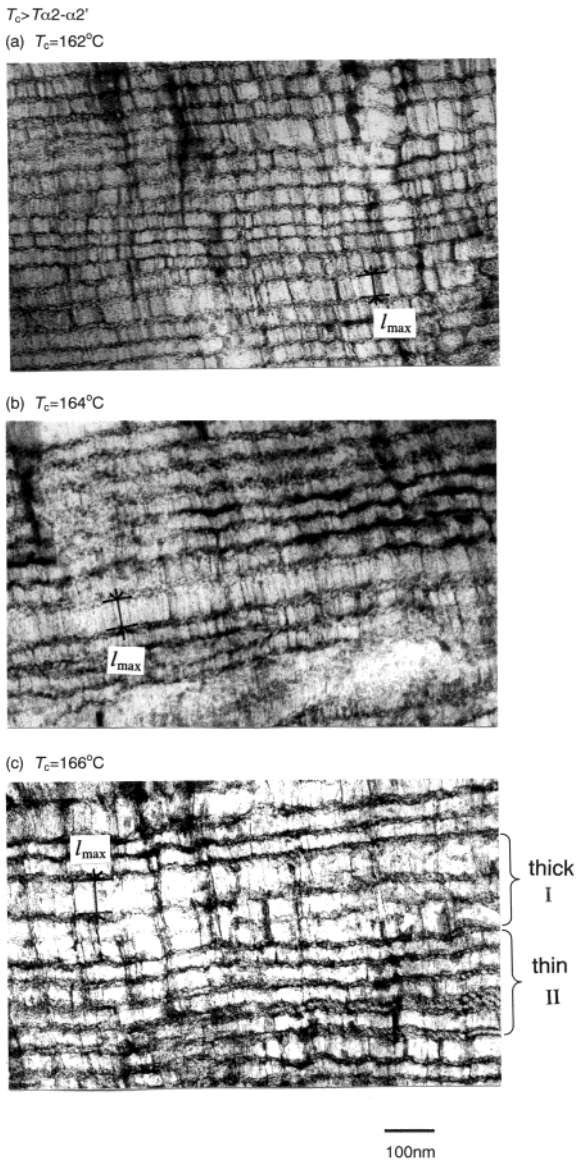

Figure 12. Transmission electron micrographs of lamellar morphology of samples crystallized at $T_c > T_{\alpha2-\alpha2'}$: (a) $T_c = 162$, (b) $T_c = 164$, and (c) $T_c = 166$ °C. Areas of thin lamellae (II) and thick lamellae (I) were indicated.

l_{max} increased slowly with increase of T_c. And at $T_c > T_{\alpha2-\alpha2'}$, l_{max} increased significantly with increase of T_c.

Breaking of the differential coefficient (dl_{max}/dT_c) was observed at $T_c = 159$°C. $T_{m,\alpha2'}$(OM) was also plotted again for comparison. T_c dependence of l_{max} showed similar tendency with that of $T_{m,\alpha2'}$(OM). The breaking temperature of dl_{max}/dT_c was in good agreement with that of $dT_{m,\alpha2'}(OM)/dT_c$. They corresponded to the $T_{\alpha2-\alpha2'}$ observed by means of wide-angle X-ray scattering and DSC. Therefore, the very high $T_{m,\alpha2'}$(OM) in α2′ phase was due to the very large l_{max}.

3.8. Equilibrium Melting Temperature. The Gibbs−Thomson plot, $T_{m,max} = T_{m,\alpha2'}$(OM) vs l_{max}^{-1}, is shown in Figure 18. $T_{m,\alpha2'}$(OM) increased linearly with decrease of l_{max}^{-1}. An experimental formula was obtained

$$T_{m,\alpha2'}(\mathrm{OM}) = 186.1 - \frac{240}{l_{max}}\ (°\mathrm{C}) \quad \text{for } M_n = 64 \times 10^3 \tag{5}$$

T_m^0 was determined as the intercept of the vertical axis

$$T_m^{\ 0} = 186.1 \pm 0.6\ °\mathrm{C} \tag{6}$$

The slope of the line, C in eq 1, was also obtained,

$$C = 240 \pm 21\ \mathrm{nm\ K} \tag{7}$$

Thus, the rigorous Gibbs−Thomson plot and T_m^0 were obtained in this study.

3.9. Validity of Gibbs—Thomson Plot Obtained by Using DSC. In this paper, the rigorous Gibbs−Thomson plot and T_m^0 were obtained by means of optical microscope. The convenient Gibbs−Thomson plot obtained by means of DSC in part 1 of this series was also shown in Figure 18. The result of convenient Gibbs−Thomson plot was similar to the rigorous one. Therefore, the validity of the convenient Gibbs−Thomson plot was confirmed. The method used to obtain the plot by means of DSC is useful as a practical and convenient one.

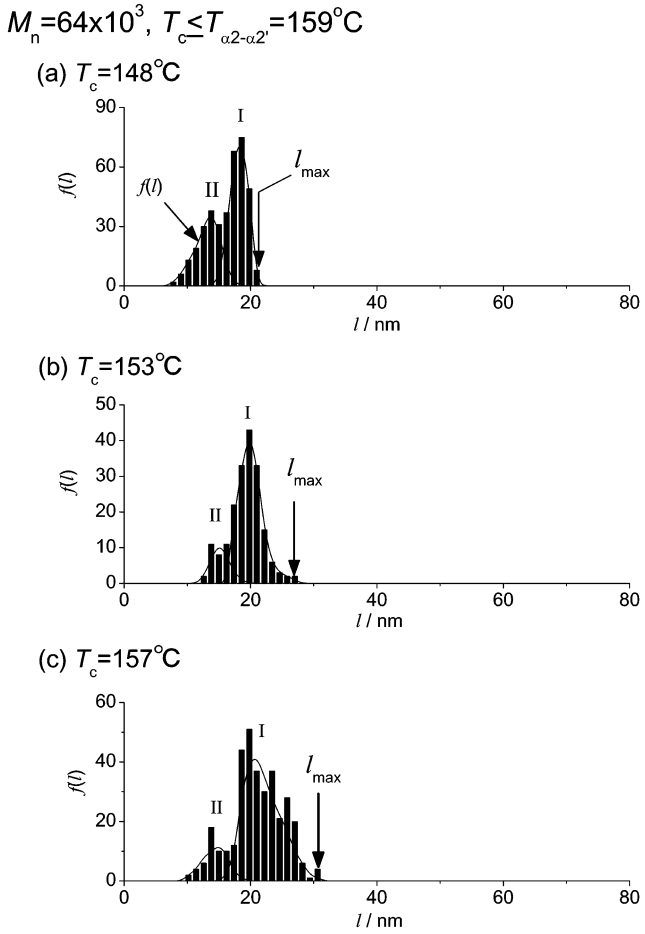

Figure 13. Histograms of lamellar thickness (l) of samples crystallized at $T_c \leq T_{\alpha2-\alpha2'}$: (a) $T_c = 148$, (b) $T_c = 153$, and (c) $T_c = 157$ °C corresponding to lamellar morphologies shown in Figure 11, parts a, b, and c, respectively. Number distributions of l ($f(l)$) were shown by solid lines. The maximum l (l_{max}) was indicated.

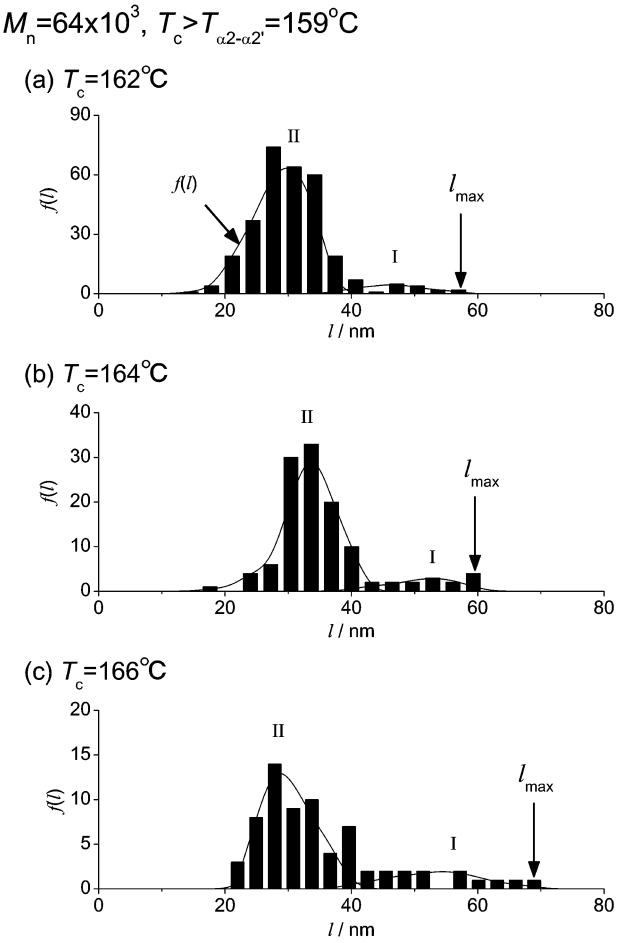

Figure 14. Histograms of lamellar thickness (l) of samples crystallized at $T_c > T_{\alpha2-\alpha2'}$: (a) $T_c = 162$, (b) $T_c = 164$, and (c) $T_c = 166$ °C corresponding to lamellar morphologies shown in Figure 12, parts a, b, and c, respectively. $f(l)$ were shown by solid lines. l_{max} was indicated.

4. Discussion

4.1. End Surface Free Energy. End surface free energy (σ_e) is obtained from C in eq 1. C is given by

$$C = \frac{2\sigma_e T_m^0}{\Delta h} \tag{8}$$

where Δh was reported as between 148 and 209 J/cm^3 in the literature.[31−36] Therefore, we obtained reliable σ_e

$$\sigma_e = (39-55) \times 10^{-7}\ \text{J/cm}^2 \tag{9}$$

Most σ_e values reported in the literature were (60−70) × 10^{-7}J/cm^2.[32−39] σ_e is obtained from the Gibbs−Thomson plot or ΔT dependence of lateral growth rate. In the former case, the Gibbs−Thomson plots used in the literature were unreliable as mentioned in part 1 of this series. In the latter case, growth rate strongly depends on ΔT. Therefore, the estimated σ_e is strongly affected by T_m^0, and the reported σ_es were not reliable because the T_m^0s of iPP in the literature were not reliable.

4.2. Broad Distribution of *l* in the α2′ Phase. Bimodal distribution of l can be explained by the forming mechanism of lamellae. Axialite with isolated mother lamellae is formed in the initial process of crystallization at high T_c. One of the authors (Hikosaka) showed that the l of the isolated mother lamellae increased linearly with crystallization time (t) (Figure 19), i.e.,

$$l = l^* + 2Ut \tag{10}$$

where U is the lamellar thickening growth rate.[40] On

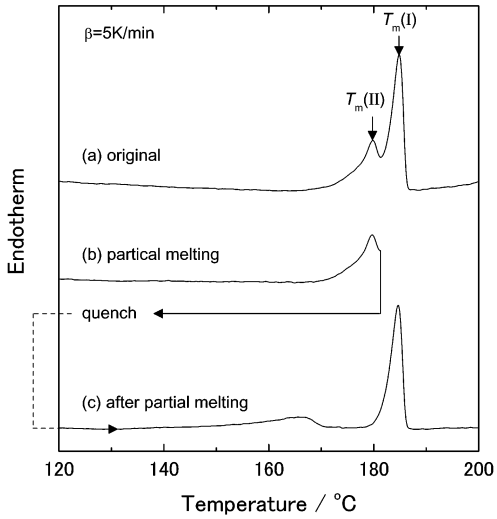

Figure 15. DSC curves of a sample crystallized at $T_c = 162$ °C: (a) original sample, (b) sample after partial melting and quench, and (c) sample after partial melting.

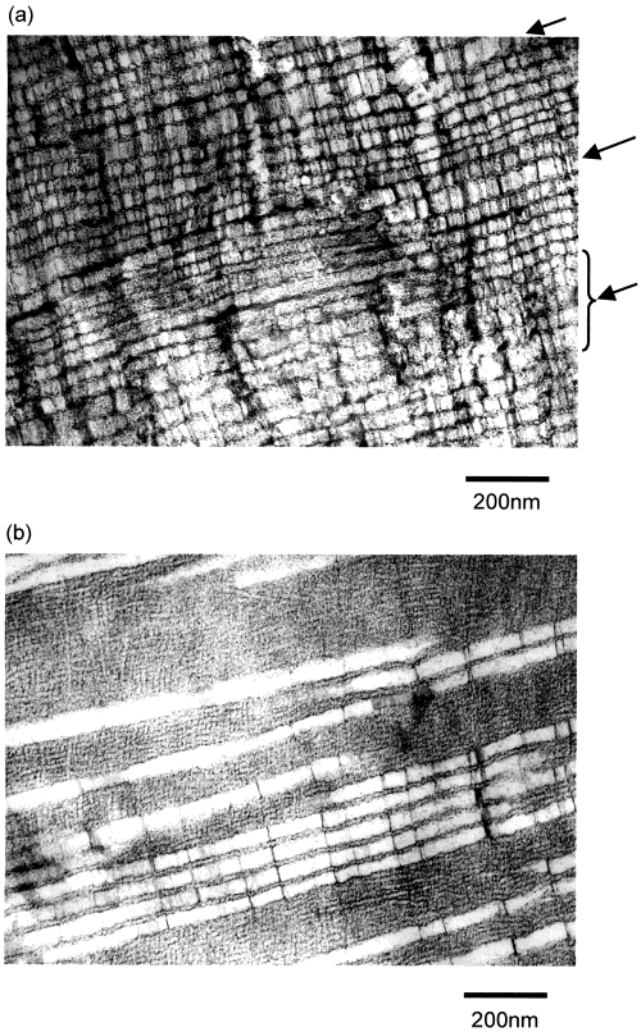

Figure 16. Typical transmission electron micrographs of iPP crystallized at T_c = 162 °C (a) before and (b) after partial melting at 181.3 °C.

the other hand, it is well-known that l of stacked lamellae are given by

$$l = l^* + W \log(t - c) \qquad (11)$$

where W is the lamellar thickening rate and c is a constant.[40] U is much larger than W.

The forming process of stacked lamellae can be explained as follows. At first, an isolated mother lamella is formed in the melt. When the end surface makes contact with the melt, significant thickening growth occurs and thick lamellae are formed. Lateral growth and thickening growth of mother lamellae occurs simultaneously.[40] After that, overgrowth starts and new daughter lamellae stack on the mother lamellae through the screw dislocation, cilia, or loop on the fold surface.[41] When a lamella is sandwiched by other lamellae, i.e., its end surface is restricted by other lamellae, it thickens with a rather slow thickening rate W. Thus, thick and thin lamellae are formed.

4.3. Test of the Assumption of the Hoffman−Weeks Plot. Figure 20 illustrates the correspondence of the Gibbs−Thomson plot and the Hoffman−Weeks plot when eq 2a is satisfied. The horizontal axes indicate ΔT and l^{-1}. It is obvious that the both plots are equivalent and give the same T_m^0 under the condition of eq 2a.

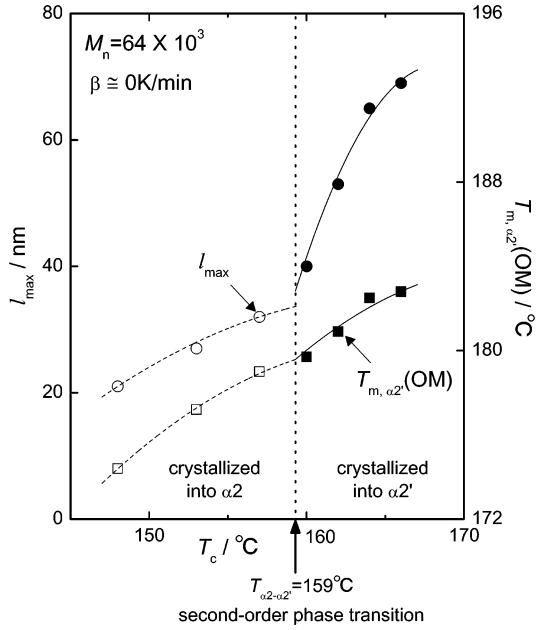

Figure 17. Plot of l_{max} and $T_{m,\alpha2'}$(OM) against T_c. l_{max} and $T_{m,\alpha2'}$(OM) of samples crystallized into α2 phase at $T_c \leq T_{\alpha2-\alpha2'}$ were indicated by open circles and squares, respectively. Those of samples crystallized into α2′ phase at $T_c > T_{\alpha2-\alpha2'}$ were indicated by filled circles and squares, respectively.

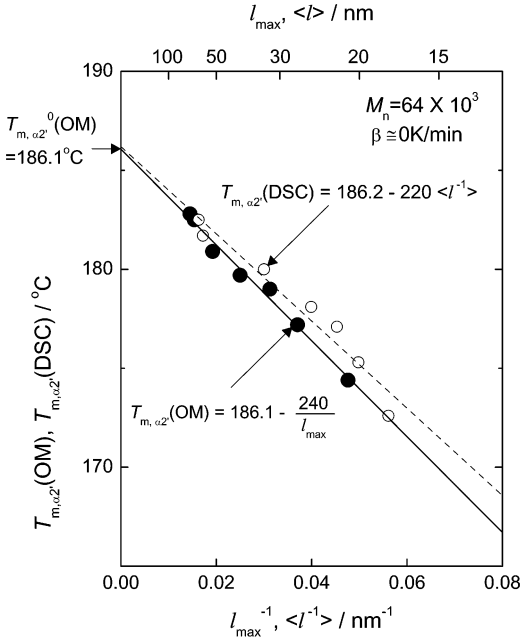

Figure 18. Gibbs−Thomson plots, $T_{m,\alpha2'}$(OM) vs l_{max}^{-1} (filled circle and solid line) and $T_{m,\alpha2'}$(DSC) vs $\langle l^{-1} \rangle$ (open circle and broken line), of iPP. The upper axis indicates l_{max} and $\langle l \rangle$.

In this section, one of the assumptions of the Hoffman−Weeks equation (eq 3a), $l \propto 1/\Delta T$ (eq 2a), was tested. The plots of l vs $1/\Delta T$ of typical polymers, such as iPP and PE, are shown in Figure 21.[41]

(a) iPP. The approximated line of l of iPP was obtained (Figure 21)

$$l = \frac{2220}{\Delta T} - 40 \text{ nm}, \quad \text{for iPP} \qquad (12)$$

The second term is large and cannot be neglected.

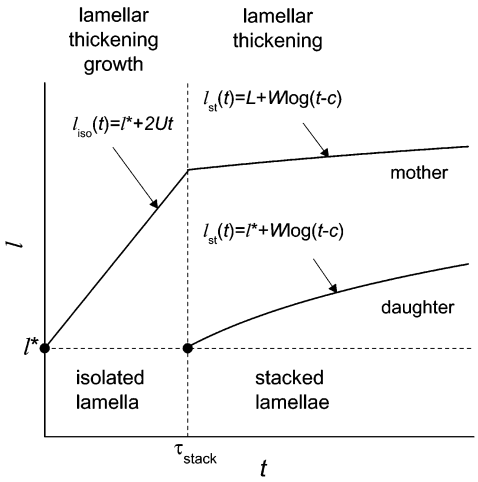

Figure 19. Increases of l of mother and daughter lamella. l^* is l of critical nucleus, τ_{stack} is onset time of stacking. The linear increase of $l(U)$ of the mother lamella changes to logarithmic increase after start of stacking. The increase of l of the daughter lamella can be shown by logarithmic function.

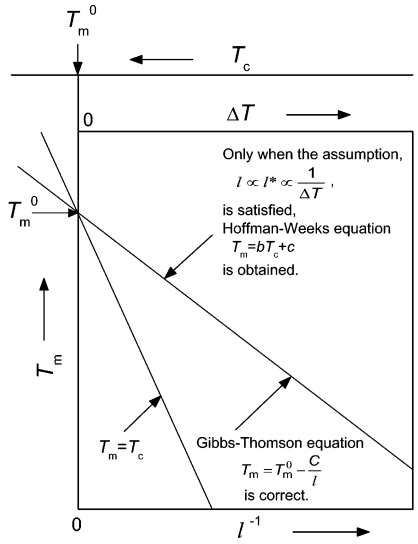

Figure 20. Hoffman−Weeks plot. It is correct only when $l \propto \Delta T^{-1}$ is satisfied. In this case, it will be shown that the Hoffman−Weeks plot becomes equivalent to the Gibbs−Thomson plot. Upper axes are T_c and ΔT, and the lower axis is l^{-1}.

Figure 22 shows the Hoffman−Weeks plot of iPP using our data. $T_{m,\alpha 2'}{}^0$ obtained by the Hoffman−Weeks plot ($T_{m,\alpha 2'}{}^0$(HW)) is

$$T_{m,\alpha 2'}{}^0(\mathrm{HW}) = 203.2\ ^\circ\mathrm{C} \tag{13}$$

$T_{m,\alpha 2'}{}^0$(HW) was 17.1 °C higher than the correct $T_{m,\alpha 2'}{}^0$(OM) as

$$T_{m,\alpha 2'}{}^0(\mathrm{HW}) = T_{m,\alpha 2'}(\mathrm{OM}) + 17.1\ ^\circ\mathrm{C} \tag{14}$$

Thus, the Hoffman−Weeks plot of iPP cannot work well.

(b) PE. In the case of PE

$$l = \frac{300}{\Delta T} + 3\ \mathrm{nm}, \quad \text{for PE} \tag{15}$$

was reported (Figure 21).[41] Therefore, the second term can be roughly neglected

$$l \cong \frac{300}{\Delta T} \propto \frac{1}{\Delta T}\,(\mathrm{nm}) \tag{16}$$

This means that eq 2a is nearly satisfied. Therefore, in the case of PE, the Hoffman−Weeks plot works.[2,23,24]

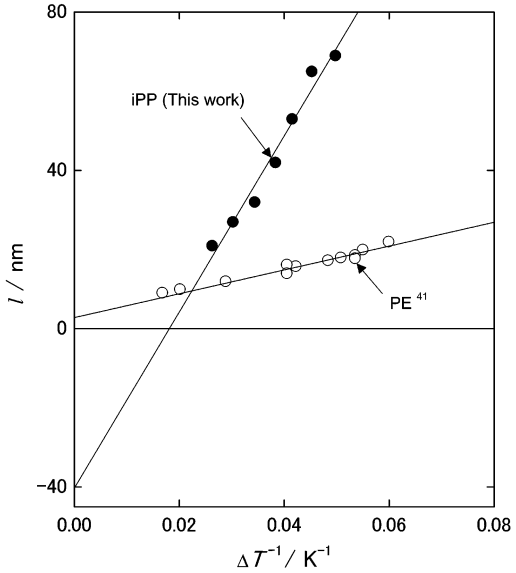

Figure 21. Plots of l against ΔT^{-1} for iPP and PE. The ΔT^{-1} dependence of l of PE was obtained by Barham et al.[41]

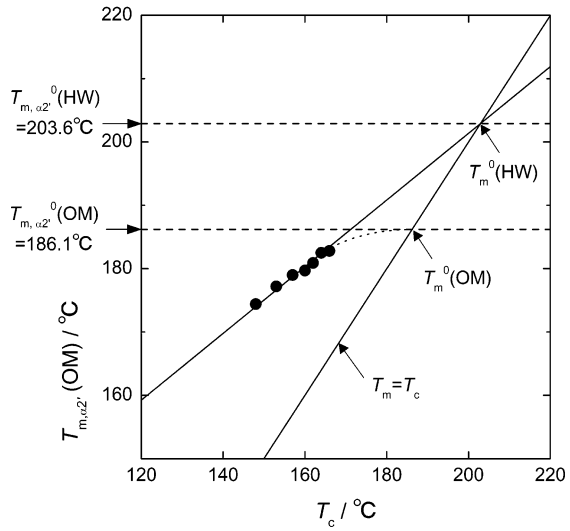

Figure 22. Hoffman−Weeks plot, $T_{m,\alpha 2'}$(OM) vs T_c, of iPP.

5. Conclusion

(1) The rigorous Gibbs−Thomson plot was obtained by using the direct correlation between $T_{m,max}$ and $l_{max}{}^{-1}$. An optical microscope and TEM were used for observations of $T_{m,max}$ and $l_{max}{}^{-1}$, respectively. The effects of the "melting kinetics" and lamellar thickening were omitted from T_m by observing the isothermal melting at $\beta \cong 0$ K/min and observing thick lamellae larger than 20 nm, respectively.

(2) The rigorous $T_{m,\alpha 2'}{}^0$ of iPP ([*mmmm*] = 99.6%, $M_n = 64 \times 10^3$) was obtained to be 186.1 °C.

(3) The $T_m{}^0$ obtained by using the convenient Gibbs−Thomson plot in part 1 of this series was similar to that obtained by using the rigorous one. Therefore, the

validity of the convenient Gibbs−Thomson plot was confirmed. The method by means of DSC is easy and useful as a practical one.

(4) It was shown that the Hoffman−Weeks plot is correct only when $l \propto 1/\Delta T$ is satisfied. In the case of iPP, $l \propto 1/\Delta T$ is not satisfied, and so the Hoffman−Weeks plot cannot work well.

(5) Breaks in differential coefficients of T_m and l against T_c were observed at $T_{\alpha 2-\alpha 2'} = 159$ °C by means of an optical microscope and TEM, respectively. Therefore, the existence of mobile phase of iPP, the α2′ phase, and the solid-to-solid transition (the α2−α2′ transition) were confirmed again.

(6) The double melting endotherm of DSC corresponded to a bimodal distribution of lamellar thickness. The broad distribution of l was explained by the mechanism of lamellar thickening growth of isolated mother lamellae and lamellar thickening of stacked daughter lamellae.

Acknowledgment. K.Y. is grateful for Dr. Ian Heritage, the General Manager of the R&D department, SunAllomer Ltd., and Mr. Hideki Tamano, the Manager of Kawasaki Development Center, SunAllomer Ltd., for their help and support.

References and Notes

(1) Part 1: Yamada, K.; Hikosaka, M.; Toda, A.; Yamazaki, S. *Macromolecules* 2003, 36, 4790.
(2) Wunderlich, B. *Macromolecular Physics*; Academic Press: New York, 1980; Vol. 3, Crystal Melting.
(3) Zhou, H.; Wilkes, G. L. *Polymer* **1997**, *38*, 5735.
(4) Toda, A.; Tomita, C.; Hikosaka, M.; Saruyama, Y. *Polymer* **1998**, *39*, 5093.
(5) Toda, A.; Hikosaka, M.; Yamada, K. *Polymer* **2002**, *43*, 1667.
(6) Fischer, E. W.; Schnidt, G. F. *Angew. Chem.*. **1962**, *74*, 551.
(7) Statton, W. O.; Geil, P. H. *J. Appl. Polym. Sci.* **1960**, *9*, 357.
(8) Hikosaka, M.; Okada, H.; Toda, A.; Rastogi, S.; Keller, A. *J. Chem. Soc., Faraday. Trans.* **1995**, *91*, 2573.
(9) Hikosaka, M.; Rastogi, S.; Keller, A.; Kawabata, H. *J. Macromol. Sci.* **1992**, *B31*, 87.
(10) Rastogi, S.; Hikosaka, M.; Kawabata, H.; Keller, A. *Macromolecules* **1991**, *24*, 6384.
(11) Gu, F.; Hikosaka, M.; Toda, S.; Ghosh, S. K.; Yamazaki, S.; Arakaki, M.; Yamada, K. *Polymer* **2002**, *43*, 1473.
(12) Maiti, P.; Hikosaka, M.; Yamada, K.; Toda, A.; Gu, F. *Macromolecules* **2000**, *33*, 9069.
(13) Janimak, J. J.; Cheng, S. Z. D.; Giusti, P. A.; Hsieh, E. T. *Macromolecules* **1991**, *24*, 2253.
(14) Norton, D. R.; Keller, A. *Polymer* **1985**, *26*, 704.
(15) Olley, R. H.; Bassett, D. C. *Polymer* **1989**, *30*, 399.
(16) Stocker, W.; Magonov, S. N.; Cantow, H.-J.; Wittmann, J. C.; Lotz, B. *Macromolecules* **1993**, *26*, 5915.
(17) Yamada, K.; Matsumoto, S.; Tagashira, K.; Hikosaka, M. *Polymer* **1998**, *39*, 5327.
(18) Alamo, R. G.; Brown, G. M.; Mandelkern, L.; Lehtinen, A.; Paukkeri, R. *Polymer* **1999**, *40*, 3933.
(19) Radhakrishnan, J.; Ichikawa, K.; Yamada, K.; Toda, A.; Hikosaka, M. *Polymer* **1998**, *13*, 2995.
(20) Hoffman, J. D.; Weeks, J. J. *J. Res. Natl. Bur. Stand. (U.S.)* **1962**, *66A*, 13.
(21) Marand, H.; Xu, J.; Srinivas, S. *Macromolecules* **1998**, *31*, 8219.
(22) Xu, J.; Srinivas, S.; Marand, H.; Agarwal, P. *Macromolecules* **1998**, *31*, 8230.
(23) Okada, M.; Nishi, M.; Takahshi, M.; Matsuda, H.; Toda, A.; Hikosaka, M.; *Polymer* **1998**, *39*, 4535.
(24) Hoffman, J. D.; Miller, R. L. *Polymer* **1997**, *38*, 3151.
(25) Cheng, S. Z. D.; Janimak, J. J.; Zhang, A.; Hsieh, E. T. *Polymer* **1991**, *32*, 648.
(26) Mezghani, K.; Phillips, P. J. *Macromolecules* **1994**, *27*, 6145.
(27) Martuscelli, E.; Silvestre, C.; Abate, G. *Polymer* **1982**, *23*, 229.
(28) Yadav, Y. S.; Jain, P. C. *Polymer* **1986**, *27*, 721.
(29) Prest, W. M., Jr.; Luca, D. J. *J. Appl. Phys.* **1975**, *46*, 4136.
(30) Prest, W. M., Jr.; Luca, D. J. *J. Appl. Phys.* **1978**, *49*, 5042.
(31) Cheng, S. Z. D.; Janimak, J. J.; Zhang, A. *Macromolecules* **1990**, *23*, 298.
(32) Krigham, W. R.; Uematsu, I. *J. Polym. Sci.* **1965**, *3*, 767.
(33) Monasse, B.; Haudin, J. M. *Colloid Polym. Sci.* **1985**, *263*, 822.
(34) Bu, H. S.; Cheng, S. Z. D.; Wunderlich, B. *Makromol. Chem. Rapid Commun.* **1988**, *9*, 75.
(35) Quirk, R. P.; Alsamarraie, M. A. A. In *Polymer Handbook*; Immergut, E. H., Ed.; John Willey & Sons: New York, 1989.
(36) Gauner, U.; Wunderlich, B. *J. Chem. Phys. Ref. Data* **1981**, *10*, 1051.
(37) Wang, Y. F.; Lloyd, D. R. *Polymer* **1993**, *34*, 2324.
(38) Lim, G. B. A.; Lloyd, D. R. *Polym. Eng. Sci.*. **1993**, *33*, 522.
(39) Clark, E. J.; Hoffman, J. D. *Macromolecules* **1984**, *17*, 878.
(40) Hikosaka, M.; Amano, K.; Rastogi, S.; Keller, A. *J. Mater. Sci.* **2000**, *35*, 5157.
(41) Barham, P. J.; Chivers, R. A.; Keller, A.; Martinez-Salazar, J.; Organ, S. J. *J. Mater. Sci.* **1985**, *20*, 1625.

MA021207A